

A mechanism for ice growth on the surface of a spherical water droplet

Yang Li,^{1,2,*} Prachi Parashar,^{3,†} Iver Brevik,⁴ Clas Persson,⁵ O. I. Malyi,^{6,7} and Mathias Boström^{7,8,‡}

¹*School of Physics and Materials Science, Nanchang University, Nanchang 330031, China*

²*Institute of Space Science and Technology, Nanchang University, Nanchang 330031, China*

³*John A. Logan College, Carterville, Illinois 62918, USA*

⁴*Department of Energy and Process Engineering,
Norwegian University of Science and Technology, NO-7491 Trondheim, Norway*

⁵*Department of Materials Science and Engineering,
KTH Royal Institute of Technology, SE-100 44 Stockholm, Sweden*

⁶*Qingyuan Innovation Laboratory, Quanzhou 362801, China*

⁷*Centre of Excellence ENSEMBLE3 Sp. z o. o., Wolczynska Str. 133, 01-919, Warsaw, Poland*

⁸*Chemical and Biological Systems Simulation Lab, Centre of New Technologies,
University of Warsaw, Banacha 2C, 02-097 Warsaw, Poland*

(Dated: March 3, 2026)

The formation and growth of ice particles, particularly on the surfaces of spherical water droplets, bear profound implications for localized weather systems and global climate. Herein, we develop a theoretical framework for ice nucleation on minuscule water droplets, establishing that $10 \sim 5000$ nm droplets can considerably increase in volume, making a substantial contribution to ice formation within mist, fog, or even cloud systems. We reveal that the Casimir-Lifshitz (van der Waals) interaction within these systems is robust enough to stimulate both water and ice growth on the surfaces of ice-cold spherical water droplets. The significant impacts and possible detectable phenomena from the curvature are demonstrated.

I. INTRODUCTION

Small ice particles, an integral element of atmospheric science, for ice-phase processes in the global hydrological cycle and precipitation¹ are known to be important, which influences weather, as well as the global climate². The size and structure of ice nuclei can influence the radiation flux in the atmosphere³, and thus weather and climate implications⁴⁻⁶. Ice nucleation is also of great importance in many other fields⁷.

Ice particles often measure less than a micrometer in diameter. These minute particles are born from a complex dance, where the water vapor adheres to and freezes on condensation nuclei diffusing throughout the cloud, fog, and mist. Consequently, it leads to the growth of intricate ice crystals. Our understanding on these phenomena is largely based on a rich tapestry of deposition theories, such as the well-established Wegener-Bergeron-Findeisen process^{2,8}. At their core, these theories posit that the inherently unstable thermodynamic equilibrium between ice and water fosters the conversion of liquid clouds into ice clouds, facilitated by the preferential accretion of water vapor onto the ice at lower moisture concentrations. Within clouds, the ice nuclei⁹, known to initially be of the order $0.1 \sim 1 \mu\text{m}$, seem to require specific surface sites to induce heterogeneous ice growth¹⁰⁻¹². On occasions, observations of higher concentrations of ice particles than expected, have been addressed with various potential explanations¹³: (i) presence of very efficient ice nucleating particles, (ii) recycling of ice in the downwelling mantle of the convective cloud, and finally (iii) through a secondary ice production process.

In this contribution, we will present a model, where Casimir-Lifshitz energies (the van der Waals interac-

tions), induced by the quantum vacuum and thermal fluctuations, can give rise to sufficiently large energies for hexagonal ice¹⁴ to grow on the surface of ice-cold submicron-sized spherical water drops. Interestingly, it is energetically favorable for the continuous growth of the internal water droplet, and for each size of the inner liquid water region, an equilibrium is found, where a micron-sized ice layer forms on the outer surface. This study uses dielectric properties of water and ice corresponding to the triple point of water¹⁵⁻¹⁷, including its relevance to mist and fog formation at or near the ground level. However, it also means, in terms of cloud systems, the model is only valid for the given conditions and may not be applicable to all clouds.

It is Elbaum and Schick^{18,19} who firstly attempted to explain ice formation on a planar water surface by emphasizing the effect due to this Casimir-Lifshitz interaction, but for planar geometry. We focus, in the current work, on the new effects from this interaction, which has not previously been predicted, and can not be predicted in the quasi planar geometry. Also, it was not until improved water and ice dielectric functions became available that Fiedler et al.¹⁵, and separately the team led by MacDowell¹⁷, predicted ice layer formation via dispersion interactions. Our work expands these works to consider the formation of ice layers on the surface of a water droplet. Notably, our prediction is that the inner surface of the ice layer (in contact with water) experiences partial premelting leading to the growth of the inner liquid water droplet, simultaneously as the outer ice surface (in contact with vapor) expands via the accumulation of water molecules from the surrounding moist. This is relevant, for instance, for water condensation in mist at conditions near the triple point of water. This is

a prediction that comes out entirely from geometry considerations. It can not be understood from past works that focused on planar geometries. (At some point the inner surface of the ice layer solidifies and the growth will then only be on the outer ice surface where dispersion forces will promote further growth of ice layer until some equilibrium is reached).

II. MODELS FOR ICE AND WATER

The parameterized dielectric functions we utilize for water and ice^{16,17} agree very well (except for at zero frequency) with the dielectric functions for discrete imaginary frequencies derived from experimental data on the real frequency axis, but they were evaluated in such a way that they do not obey the Kramers-Kronig relation (causality). In contrast, the water model by Fiedler, Parsons and co-workers¹⁵ was fitted directly on the real frequency axis and obeys causality. The zero-frequency dielectric constants for water and ice are adjusted based on experimental data. These data sets established on experiments^{16,17} present, unlike the data used in the past^{19,20}, only one crossing between the curves for ice and water dielectric functions at imaginary frequencies. This will have far-reaching consequences for our prediction of a Wegener-Bergeron-Findeisen mechanism of ice growth in low-lying clouds, mists and fogs.

III. CASIMIR-LIFSHITZ FREE ENERGY FOR THE CONCENTRIC SPHERE GEOMETRY

In Ref. [20], Parashar, Shajesh, and their coworkers demonstrated that the variation of the Casimir-Lifshitz interaction (CL) energy, excluding the self-energy part, can be computed for layered concentric spherical ice particles. It should be mentioned that divergences usually plague the Casimir self-energy, including the bulk and surface contributions, of a single spherical body. This was made clear by K. A. Milton²¹, P. Candelas²², and analyzed by, for instance, I. Brevik et al.²³ some years ago. As shown by some of our authors, the divergences inside and outside the spherical surface are indeed cancelled out exactly, when the refractive indices on two sides of the surface are equal²³. Similar argument is even applied to cylinder case²⁴. But typically this cancellation is not available. These divergences keep raising controversies up to recently^{25,26}, and a satisfactory method to deal with these divergences is still in need^{27,28}. In this paper, however, we study the mechanism due to the Casimir-Lifshitz interaction between two media intermediated via a third medium, with two surfaces involved and no divergence occurring at all. The potential effects related to those divergences will be a novel topic for our studies in the near future.

For submicron-sized water droplets, we predict that the results are dramatically modified due to the curved

spherical geometry. For full details of the theory for concentric sphere Casimir-Lifshitz free energy applied to ice-water systems, we refer to Ref. [20] and the references therein. With the inner and outer ice layer radii labeled a and b as shown in Fig. 1a, the CL energy due to the transverse magnetic (TM) modes F_H is written as

$$F_H = T \sum_{n=0}' \sum_{l=1}^{\infty} 2\nu \ln[1 - r_{32}^H(n, l; b) r_{21}^H(n, l; a)], \quad (1)$$

where $\nu = l + 1/2$, and the primed sum indicates that the first static term ($n = 0$) should be weighted in half. The scattering coefficients are given by

$$r_{32}^H(n, l; b) = \frac{[e_l(\kappa_{3;n}b), e_l(\kappa_{2;n}b)]_{\varepsilon}}{[e_l(\kappa_{3;n}b), s_l(\kappa_{2;n}b)]_{\varepsilon}}, \quad (2a)$$

$$r_{21}^H(n, l; a) = \frac{[s_l(\kappa_{2;n}a), s_l(\kappa_{1;n}a)]_{\varepsilon}}{[e_l(\kappa_{2;n}a), s_l(\kappa_{1;n}a)]_{\varepsilon}}, \quad (2b)$$

in which $\kappa_{i;n} = 2\pi n T \sqrt{\varepsilon_i \mu_i}$, $i = 1, 2, 3$ (with the indices corresponding to water, ice, vapor respectively), the temperature $T = 273.16$ K, and the bracket $[\cdot, \cdot]_{\varepsilon}$, involving the permittivity ε , is defined as

$$[f(x), g(x)]_{\varepsilon} = \frac{f'(x)}{\varepsilon_f} g(x) - f(x) \frac{g'(x)}{\varepsilon_g}. \quad (3)$$

$e_l(x) = \sqrt{2x/\pi} K_{\nu}(x)$ and $s_l(x) = \sqrt{\pi x/2} I_{\nu}(x)$, with $K_{\nu}(x)$ and $I_{\nu}(x)$ being the modified spherical Bessel functions. The transverse electric (TE) CL free energy, which will be studied as the representative quantity in the Appendix, is obtained with the substitutions $H \rightarrow E$, $\mu \leftrightarrow \varepsilon$. For nonmagnetic dielectrics, the $n = 0$ terms can be explicitly written as $F_E^{n=0} = 0$ and

$$F_H^{n=0} = T \sum_{l=1}^{\infty} \nu \ln \left[1 + \frac{(\varepsilon_3 - \varepsilon_2)(\varepsilon_2 - \varepsilon_1)}{(\frac{l+1}{l}\varepsilon_3 + \varepsilon_2)(\varepsilon_2 + \frac{l}{l+1}\varepsilon_1)} \left(\frac{a}{b}\right)^{2\nu} \right], \quad (4)$$

where ε_i takes its static value. The impacts of the spherical geometry are evident even for the relatively simple static part, implying their significance as shown in the following limiting cases.

Suppose the separation between inner and outer interfaces $d = b - a$ goes to zero with a remaining constant. Then in this limit, the retardation effects are too trivial to be included, and only non-retarded contributions survive. The TM CL energy, as an instance, in this case is

$$F_H = -4\pi a^2 \frac{A}{12\pi d^2}, \quad d \rightarrow 0, \quad (5)$$

where A is the Hamaker constant of the corresponding planar three-layer configuration. (See the Appendix for detailed calculation of TM CL energy.) We thus claim that in this small-separation limit, the CL interaction in the concentric configuration is just the same as that

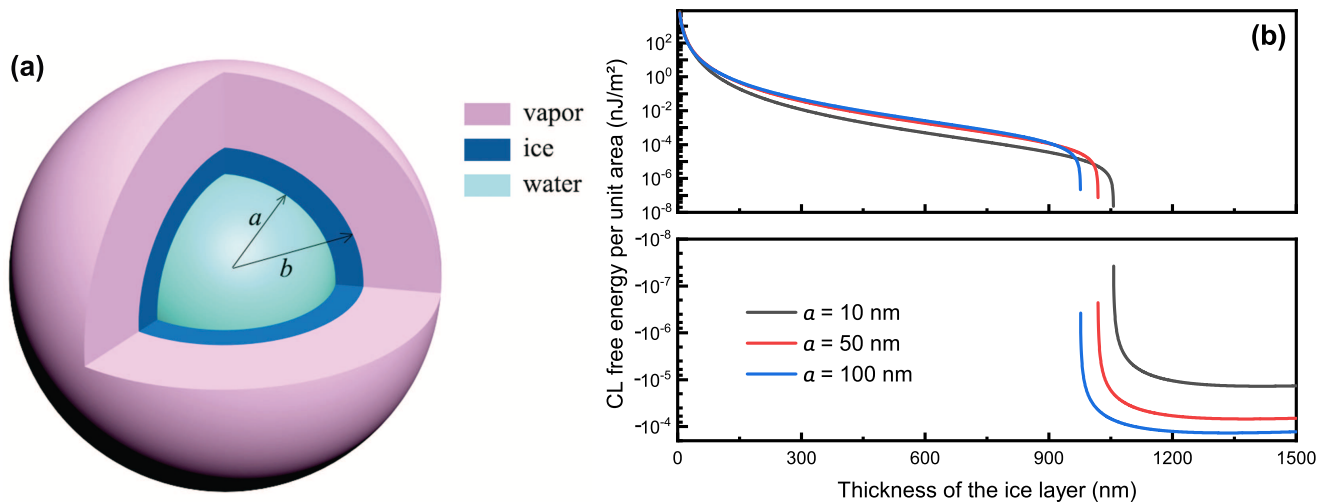


Figure 1. (a) The schematic illustration on the configuration studied, i.e., the water-ice-vapor spherical system, with the inner and outer radius of the ice layer being a and b . (b) The Casimir-Lifshitz free energy per unit area as a function of the thickness of the ice layer, i.e., the difference between the outer b and inner a radius of the intervening layer in the water-ice-vapor concentric configuration.

in the planar case. It is not a surprising result, since at a very small separation the local interaction dominates, meaning that the impacts due to the geometry are negligible. However, it happens only when the separation is extremely small. Generally within the scale where the continuum theory is valid, the retardation effects are highly nontrivial, as shown in the Appendix. Therefore, the retardation, even in our case where the size of the configuration may look small, should play an important role.

Even if the retardation is fully counted, the geometry of the configuration acts as another factor making the situation more complicated. In contrast with the small-separation limit above, if $d = b - a$ kept constant but $a \rightarrow \infty$ (referred to as the “planar limit” here), then TM Casimir-Lifshitz free energy F_H , based on the Appendix, behaves as

$$\frac{F_H}{4\pi a^2} = T \sum_{n=0}^{\infty} \int_0^{\infty} \frac{dk k}{2\pi} \ln \left(1 + \frac{\varepsilon_2 \tilde{\kappa}_{3,n} - \varepsilon_3 \tilde{\kappa}_{2,n}}{\varepsilon_2 \tilde{\kappa}_{3,n} + \varepsilon_3 \tilde{\kappa}_{2,n}} \times \frac{\varepsilon_1 \tilde{\kappa}_{2,n} - \varepsilon_2 \tilde{\kappa}_{1,n}}{\varepsilon_1 \tilde{\kappa}_{2,n} + \varepsilon_2 \tilde{\kappa}_{1,n}} e^{-2\tilde{\kappa}_{2,n} d} \right), \quad (6)$$

in which $\tilde{\kappa}_{i,n} = \sqrt{k^2 + \varepsilon_i \zeta_n^2}$, and the famous Dzyaloshinskii-Lifshitz-Pitaevskii (DLP) formula for the CL free energy per unit area of the planar three-layer configuration^{29,30} is exactly derived. The same arguments apply to the TE contribution. According to Eq. (20), the impacts due to the geometry, which are embodied in the curvature characterized by the factor a , vanish as a approaches infinity. This result is consistent with the assumption usually employed, that is, for a relatively large medium, the Casimir-Lifshitz interaction near its surface can be evaluated in terms of the planar configuration. As directly shown below, the effects of curvature

here can only be fully eliminated by decreasing the curvature, provided the separation between interfaces are not extremely small. In this sense, our analysis demonstrates the importance of understanding curvature effects for submicron-layered systems.

Given that the analytical investigation as above is not generally available because of the complex forms of permittivities of real materials, we mainly resort to numerical evaluations to unveil corresponding phenomena and physics. Results will be presented for the concentric sphere geometry with inner radii ranging from 10 nm to 1 μm , exactly in the size range of observed ice nuclei discussed in the introduction.

IV. RESULTS AND DISCUSSIONS

It was recently predicted that minimization of Casimir-Lifshitz free energies could induce ice layer formation at the surfaces of water^{15–17}, as well as on AgI particles in clouds¹⁶. The mechanism for ice formation has also been invoked for self-preservation of gas hydrates³¹. However, all those works, predicting the minimization of free energy with the ice growth, exploited theories with the planar approximation, which in the submicron size, are often better described as concentric spherical systems. The study on energies in the actual submicron concentric spherical systems unveils interesting new physics. The CL free energy curves as functions of the ice layer thickness, for water droplets with given inner radii ($a = 10, 50, \text{ and } 100 \text{ nm}$), are shown in Fig. 1b. Two things are of immediate interest. Firstly, the depth of the minimum for the free energy per unit area increases, as the water droplet radius increases. It follows from energy considerations that close to micron-thick ice layers grow

on nano-sized water droplets under the right conditions. Thereafter, the inner liquid core of the layered droplet grows at the expense of the inner parts of the ice coating. The ice film thickness, in turn, is kept close to constant by water vapor adsorption, leading to an expanding inner radius (a) and thus the radius of the composite nuclei (b). Notably, with a thinner ice layer, it is not energetically favorable for the water droplet to grow since the energy increase with increasing a for small ice layer thicknesses. The second important observation is that the relative amount of ice in the droplet, which minimizes the energy, increases with decreasing water droplet radius. As can be seen in Table I, the relative amount of ice growth is predicted to be dramatic for nano-sized water droplets. This leads us ultimately to predict an enhanced ice growth mechanism for ice nucleating nano-droplets. This occurs in a new “secondary” way, via a reduced CL free energy, that leads to the simultaneous growth of both the interior water droplet and the ice coating with the adsorption of water molecules from the vapor phase. This results in larger volumes of ice, but should not be mixed up with the traditional secondary ice processes. Furthermore, the planar approximation, compared with a water droplet of a radius 10 nm, gives a correct order of magnitude estimate for the predicted ice coating thickness. It should be emphasized that for a fixed water droplet size, the repulsive Casimir-Lifshitz stress can be substantially increased below the equilibrium ice film thickness. This can lead to the establishment of the initial growth of an ice layer due to dispersion energies.

Moreover, we see a minimum equilibrium thickness of ice layer, when varying the inner radius a , as demonstrated by Fig. 2a. The red dot there marks the minimum thickness of ice layer at 1020 nm with a being about 2642 nm. However, the minimum of the Casimir-Lifshitz free energy per unit area, shown as the black dot in Fig. 2a, deviates from the minimum thickness. This small deviation is due to the combination of the size of the sphere and the free energy per unit area. It should be noted that the CL free energy of the spherical system, instead of the CL free energy per unit area as in planar cases, should be minimized to achieve the stability of the system. The total Casimir-Lifshitz free energy in this system does not show a minimum. The CL free energy per unit area here, which is defined as the total free energy divided by the area of the inner interface, is employed to compare with the corresponding planar case, while the CL free energy itself decreases monotonically as the size of the sphere increases, since the planar case is approached then. (See Table I for numbers showing this tendency.)

Although in the considered range of water droplet sizes, the CL free energy is minimized for ice layer thicknesses of same order of magnitude as was predicted for a planar water surface^{15–17}, the impact of curvature demonstrates itself by the variation of the ice layer thickness within several hundreds of nanometers. In Fig. 2b, we demonstrate that for relatively thin ice layers, the CL

a (nm)	ice thickness (nm)	F_{\min} (nJ/m ²)	volume ratio (%)
10	1415	-1.38×10^{-5}	2.89×10^8
20	1405	-2.75×10^{-5}	3.62×10^7
40	1386	-5.50×10^{-5}	4.53×10^6
60	1368	-8.23×10^{-5}	1.35×10^6
80	1351	-1.09×10^{-4}	5.72×10^5
100	1334	-1.36×10^{-4}	2.94×10^5
200	1262	-2.66×10^{-4}	3.90×10^4
400	1163	-4.88×10^{-4}	5.87×10^3
600	1106	-6.51×10^{-4}	2.20×10^3
800	1072	-7.61×10^{-4}	1.18×10^3
1700	1025.18	-9.31×10^{-4}	3.12×10^2
2500	1020.18	-9.34×10^{-4}	1.79×10^2
3000	1020.39	-9.20×10^{-4}	1.41×10^2
3500	1021.32	-9.04×10^{-4}	1.16×10^2
4000	1022.52	-8.88×10^{-4}	9.80×10^1
5000	1025.26	-8.58×10^{-4}	7.50×10^1
5500	1026.14	-8.45×10^{-4}	6.71×10^1
∞	1043.84	-6.19×10^{-4}	—

Table I. The equilibrium ice layer thickness at minima for the free energy per unit area F_{\min} (for inner surface of ice layer) as a function of water droplet radius (a). We also present in the table the droplets’ relative volume growth due to ice layer formation in percentage ($100 \times (b^3 - a^3)/a^3$ %).

free energy per unit area enhanced due to the curvature approaches the planar approximation for $a \geq 100$ nm. The enhancement is weaker for thinner ice layer. Besides, with the varying a , the enhancement with respect to its planar counterpart is not monotonic, since the interaction between the inner and outer surfaces of the ice layer drastically decays as the size of water ball goes to zero. For thicker ice layers, as shown in Fig. 2c, more complicated dependencies on a are observed. When the ice layer is still relatively thin, $b - a = 0.5 \mu\text{m}$, similar behavior as in Fig. 2b is seen. With larger thicknesses, the speed of converging to the planar case is typically small. In addition, a dip, which is particularly apparent for $b - a = 0.75 \mu\text{m}$, appears, since the CL free energy of planar case for scaling changes sign. The curvature tends to raise the CL free energy, but if the surfaces are too far away from each other and the inner surface is too small, a strong enough interaction can hardly be maintained.

Table I also shows us the predicted decreasing ice-water ratio, as the radius of the inner surface of ice layer increases, which implies a particularly noticeable growth-promoting effect for small water drops. This result, in the larger perspective, displays a “secondary” ice growth mechanism that should be important enough to have meteorological impacts. As demonstrated in the first half of the 20th century^{2,8} by Wegener, Bergeron, and Findeisen, mixtures of ice and water are thermodynamically unstable. Here, our prediction is that the interior water droplet is in contact with a micron-sized ice layer.

Therefore, in subsequent steps, the inner, unfrozen, water droplet core (in contact with ice) will eventually freeze, but the droplet ends up substantially larger compared to the case when only the initial water droplet had frozen.

Notably, Mie scattering of light against ice-coated water droplets depends on both the relative amounts of water and ice, as well as or more importantly, the nuclei sizes. This means the predicted effect is already part of our daily life, when we ponder the colors of the sky. A very useful way of measuring particle size is to make use of Mie scattering. Consider a plane wave of intensity I_0 falling towards a uniform dielectric sphere of radius a and refractive index n . The Mie scattering formalism is valid for all values of b relative to the wavelength λ of the incident light, but we will here confine ourselves to the Rayleigh approximation, which holds when the size of the sphere is much smaller than the wavelength. In practice, this means that the Rayleigh approximation is useful for $b < \lambda/10$, or approximately $b < 50$ nm in optics. Infrared radiation, notably, is between 780 nm and 1 mm. Then, the intensity I observed at a distance R away from the scatterer is

$$I = I_0 \frac{1 + \cos^2 \theta}{2R^2} \left(\frac{2\pi}{\lambda} \right)^4 \quad (7)$$

where θ is the scattering angle. This expression shows that I is very sensitive versus variations in size of the layered water droplet. As the system grows, this leads to many orders of magnitude corrections for the scattered intensity. A more accurate approach would be to use Mie (or Rayleigh) theory for stratified fluid spheres³², which makes it possible to incorporate the difference between the refractive indices for ice and water. In practice, this additional refinement would hardly be of any importance, however, as these refractive indices are so similar.

V. CONCLUSIONS

Herein, we yield novel insights into coupled ice formation and premelting processes, emphasize the crucial role of accurate material parameterization and geometry, and shed light on the role of Casimir-Lifshitz interactions. As shown in the current letter, within appropriate geometry and using energy considerations, micron-thick ice layers grow on nano-sized spherical water droplets under the right conditions. Thereafter we predict the inner liquid core of the layered droplet to grow at the expense of the inner parts of the ice coating. The ice film thickness, in turn, is kept close to constant by the condensation, and subsequent freezing, of water vapor at the outer ice surface. The thermodynamic instability inherent in ice-water mixtures then leads to the eventual freezing of the interior unfrozen water droplet. The resulting ice droplet is substantially larger than predicted if solely the initial water droplet had frozen, challenging conventional understandings of ice formation. A noteworthy aspect of this mechanism is the Mie scattering of

light against ice-coated water droplets, which is directly impacted by the relative proportions of water/ice and the size of the nuclei. Intriguingly, this effect permeates into everyday life, subtly influencing the colors we see. These findings unsettle previous predictions and authenticate the formation of a micron-sized ice layer on the surface of cold water, a stark contradiction to prior assumptions of premelting. Recently, a complex spectrum of interactions³³ and stability states in our exploration of planar three-layer and four-layer scenarios³⁴ are discovered. Together with the important influences from the geometry, diverse ice premelting and formation phenomena in more complicated systems are anticipated.

Our analysis does operate on certain assumptions, such as the insignificance of surface charge and surface adsorption of free ions³⁵. At low salt concentrations and pH around 7, this is expected to be a useful approximation, but may gloss over some potentially pivotal aspects of ice formation and premelting processes (e.g. pH effects from sulfur in the atmosphere from volcanoes³⁶), indicating the need for further research to decipher charge-induced interactions^{37,38}. We also point out that the interfacial tension of the droplet is related to attractive forces in the interface region, which are only partially encompassed by the van der Waals energies. There would be effects from the size-dependence of surface tension of the curved water-vapor interface. Pruppacher and Klett gave a quasi-thermodynamical relation between radius and changes in surface tension³⁹,

$$\sigma_{w/v} = \frac{\sigma_{w/v}(\infty)}{1 + (2/a)\Gamma_w^{w/v}/(\rho_w - \rho_v)}, \quad (8)$$

where $\sigma_{w/v}$ is water-vapor surface tension at radius a , $\sigma_{w/v}(\infty)$ the surface tension for a planar water-vapor interface, $\Gamma_w^{w/v}$ the Gibbs adsorption, and $\rho_w - \rho_v$ is the difference in the mass densities of water and vapor. Future research should also address various other related factors, including the dynamics of water molecules, to constrain the relevant nucleation parameters⁴⁰.

APPENDIX: LIMITING BEHAVIORS

Suppose the separation between the inner and outer interface $d = b - a$ goes to zero, while a is kept constant. Obviously, in the zero-separation case, $d = 0$, the Casimir free energy in the concentric configuration diverges, as the corresponding case in the planar system. To capture its small-separation behaviors, we consider the separation nonzero, but infinitely small, that is, the TM Casimir free energy per unit area with respect to the inner interface, for instance (TE part following the same arguments), expressed as

$$f_{\text{H,s}} = \frac{T}{4\pi a^2} \sum_{n=0}^{\infty} \sum_{l=1}^{\infty} 2\nu \ln[1 - r_{32}^{\text{H}}(n, l; b)r_{21}^{\text{H}}(n, l; a)], \quad (9a)$$

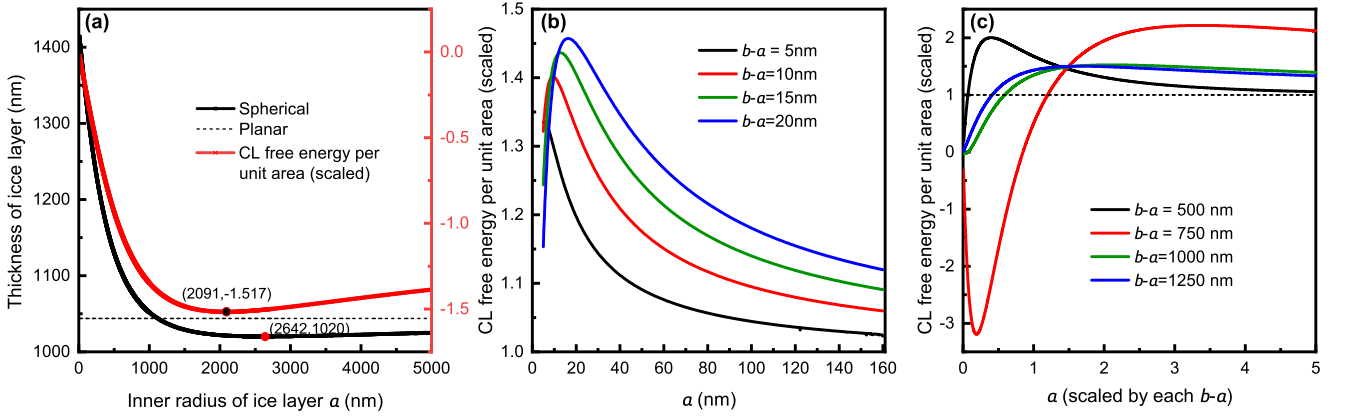


Figure 2. (a) The thickness of the ice layer (solid line) minimizing the CL free energy per unit area as a function of droplet's inner radius a . The global minimum thickness is about 1020 nm located near $a = 2642$ nm (red dot). The minimum thickness of the ice layer in the corresponding planar configuration is also shown (dotted line) as a reference. The minimum CL free energy per unit area for each a , scaled by the absolute value of that for the planar case, are plotted as the red line, with the black dot being the minimum. (b) With small ice layer thicknesses, the CL free energy per unit area of the concentric configuration, scaled by their corresponding planar cases with the same ice layer thicknesses, as the function of a . (c) The plot is in the same manner as (b) except for the relatively large ice layer thicknesses.

in which $b = a + d$, $\nu = l + 1/2$, functions $e_l(x)$ and $s_l(x)$ are defined and utilized as in the main text, and

$$r_{32}^H(n, l; b) = \frac{[e_l(\kappa_{3;n}b), e_l(\kappa_{2;n}b)]_\varepsilon}{[e_l(\kappa_{3;n}b), s_l(\kappa_{2;n}b)]_\varepsilon}, \quad (9b)$$

$$r_{21}^H(n, l; a) = \frac{[s_l(\kappa_{2;n}a), s_l(\kappa_{1;n}a)]_\varepsilon}{[e_l(\kappa_{2;n}a), s_l(\kappa_{1;n}a)]_\varepsilon}, \quad (9c)$$

In the small-separation limit $d \rightarrow 0_+$, the $n = 0$ contributions are expressed as

$$\tilde{f}_{H,s}^{n=0} \sim \frac{T}{4\pi a^2} \sum_{l=1}^{\infty} \nu \ln \left[1 + \frac{(\varepsilon_3 - \varepsilon_2)(\varepsilon_2 - \varepsilon_1)e^{-\frac{2\nu}{a}d}}{\left(\frac{l+1}{l}\varepsilon_3 + \varepsilon_2\right)(\varepsilon_2 + \frac{l}{l+1}\varepsilon_1)} \right], \quad (10)$$

where the leading order in $(a/b)^{2\nu} = e^{-2\nu \ln(1+d/a)} \approx e^{-2\nu d/a}$ for arbitrarily ν is used, since $d/a \rightarrow 0$ is the smallest dimensionless scale involved here. For the planar limit, the Casimir free energy per unit area due to the $n = 0$ contribution is written as

$$\begin{aligned} \tilde{f}_{H,p}^{n=0} &\sim \frac{T}{2} \int_0^\infty \frac{dkk}{2\pi} \ln \left[1 + \frac{(\varepsilon_3 - \varepsilon_2)(\varepsilon_2 - \varepsilon_1)}{(\varepsilon_3 + \varepsilon_2)(\varepsilon_2 + \varepsilon_1)} e^{-2kd} \right] \\ &= -\frac{A_0}{12\pi d^2}, \end{aligned} \quad (11)$$

where A_0 is the $n = 0$ Hamaker constant of the corresponding planar three-layer configuration. It is demonstrated that for a general inner radius a , $\tilde{f}_{H,s}^{n=0}$ behaves differently from its planar counterpart. The most evident deviations are seen for relatively small angular index l , and as l increases, the corresponding planar results are approached, since the differences between $\frac{l+1}{l}\varepsilon_3$, $\frac{l}{l+1}\varepsilon_1$ and ε_3 , ε_1 in the denominator in Eq. (10) vanish.

For $n > 0$ contributions, the similar behaviors are observed. For planar case, in the small-separation limit, where the retardation is not significant, the contribution from the n th ($n > 0$) order of Matsubara frequency to the Casimir free energy per unit area is expressed as

$$\tilde{f}_{H,p}^n = \frac{T}{2\pi d^2} \int_0^\infty dkk \ln \left[1 + R_{321}^{(p)}(n) e^{-2k} \right]. \quad (12)$$

where the factor $R_{321}^{(p)}(n)$ is

$$R_{321}^{(p)}(n) = \frac{\varepsilon_3(i\zeta_n) - \varepsilon_2(i\zeta_n)}{\varepsilon_3(i\zeta_n) + \varepsilon_2(i\zeta_n)} \frac{\varepsilon_2(i\zeta_n) - \varepsilon_1(i\zeta_n)}{\varepsilon_2(i\zeta_n) + \varepsilon_1(i\zeta_n)}. \quad (13)$$

In terms of the similar form, we can write the contribution for the concentric configuration corresponding to Eq. (12), in the small-separation limit, as

$$\tilde{f}_{H,s}^n = \frac{T}{2\pi d^2} \sum_{l=1}^{\infty} \frac{\nu d^2}{a^2} \ln \left[1 + R_{321}^{(s)}(n, l; a) e^{-\frac{2\nu}{a}d} \right], \quad (14)$$

where the correspondence $d/a \rightarrow dk$, $\nu d/a \rightarrow k$ as above can be applied. To explicitly figure out $R_{321}^{(s)}(n, l; a)$, it is observed that large orders of l contribute most significantly, which means the uniform asymptotic expansion (UAE) can be employed⁴¹. Then the functions $e_l(x)$ and $s_l(x)$ are approximated as

$$e_l(x) \sim \frac{\sqrt{z}e^{-\nu\eta(z)}}{(1+z^2)^{\frac{1}{4}}}, \quad s_l(x) \sim \frac{\sqrt{z}e^{\nu\eta(z)}}{2(1+z^2)^{\frac{1}{4}}}, \quad (15a)$$

$$e'_l(x) \sim \frac{e^{-\nu\eta(z)}(1+z^2)^{\frac{1}{4}}}{-\sqrt{z}}, \quad s'_l(x) \sim \frac{e^{\nu\eta(z)}(1+z^2)^{\frac{1}{4}}}{2\sqrt{z}}, \quad (15b)$$

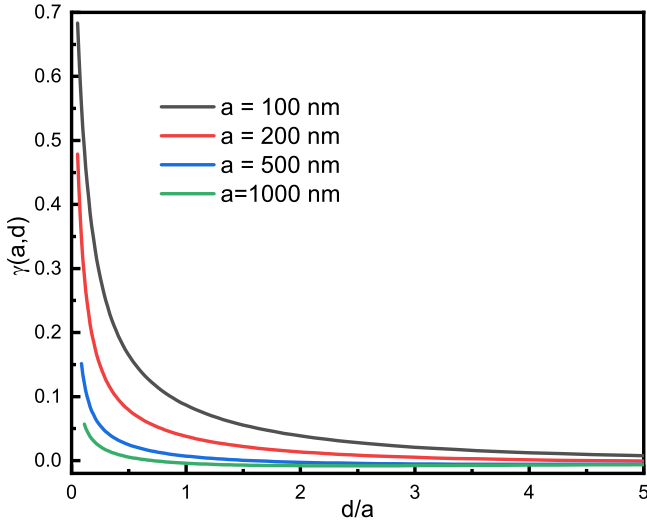


Figure 3. The factor $\gamma(a, d)$ defined in Eq. (18) as a function of d/a for each given inner radius $a = 100\text{nm}$ (black), $a = 200\text{nm}$ (red), $a = 500\text{nm}$ (blue), and $a = 1000\text{nm}$ (green).

where z and $\eta(z)$ are $z = x/\nu$ and

$$\eta(z) = \sqrt{1+z^2} + \ln \frac{z}{1+\sqrt{1+z^2}}. \quad (15c)$$

We are thus led to ($z_{i,x} = \sqrt{\varepsilon_i} \zeta_n x/\nu$)

$$r_{32}^H(n, l; b) \sim \frac{\varepsilon_2(1+z_{3,b}^2)^{1/2} - \varepsilon_3(1+z_{2,b}^2)^{1/2}}{\varepsilon_2(1+z_{3,b}^2)^{1/2} + \varepsilon_3(1+z_{2,b}^2)^{1/2}} \frac{2}{e^{2\nu\eta(z_{2,b})}}, \quad (16a)$$

$$r_{21}^H(n, l; a) \sim \frac{\varepsilon_1(1+z_{2,a}^2)^{1/2} - \varepsilon_2(1+z_{1,a}^2)^{1/2}}{\varepsilon_1(1+z_{2,a}^2)^{1/2} + \varepsilon_2(1+z_{1,a}^2)^{1/2}} \frac{e^{2\nu\eta(z_{2,a})}}{-2}, \quad (16b)$$

which result in the $-r_{32}^H(n, l; b)r_{21}^H(n, l; a)$ with $d \rightarrow 0_+$ expressed as

$$-r_{32}^H(n, l; b)r_{21}^H(n, l; a) \sim \frac{\varepsilon_2 - \varepsilon_3}{\varepsilon_2 + \varepsilon_3} \frac{\varepsilon_1 - \varepsilon_2}{\varepsilon_1 + \varepsilon_1} e^{-2\nu d/a}. \quad (17)$$

Therefore, in the small-separation limit, $R_{321}^{(s)}(n, l; a)$ approaches $R_{321}^{(p)}(n)$, and the distinction between the spherical and planar geometries disappears. Evidently, the same arguments applies to the TE contributions.

As a glimpse of the importance of the retardation, we compare the Casimir free energy per unit area for the water-ice-vapor concentric configuration, with the corresponding small-separation value where the retardation can be ignored, that is,

$$\gamma(a, d) \equiv -\frac{12\pi d^2 f_{H,s}(a, d)}{A}, \quad (18)$$

in which A is the total Hamaker constant. In Fig. 3, $\gamma(a, d)$ is shown for some fix inner radius. When d/a is large, meaning that the separation d can not be considered small in any sense, the discrepancy between the

retarded and non-retarded free energy is manifest. Even d/a approaches to a relatively small value about 0.05, the distinction is still obvious, especially when a is large. This result is natural, since the retardation can be ignored only if the absolute value of the separation is small. Therefore, even the concentric system might be tiny (in the hundreds or even tens of nanometer scale), the retardation can hardly be ignored.

On the other way round, when $d = b - a$ kept constant but $a \rightarrow \infty$, we arrive at another limiting case (or referred to as the ‘‘planar limit’’). Surprisingly, the UAE is also appropriate to be employed to investigate behaviors in this limit²⁰. Then the arguments above can be directly followed, except for the term $-r_{32}^H(n, l; b)r_{21}^H(n, l; a)$ in the instance above, which can be calculated, given $a \rightarrow \infty$, as

$$\begin{aligned} & e^{-2\nu\eta(z_{2,b})+2\nu\eta(z_{2,a})} \frac{\varepsilon_2(1+z_{3,b}^2)^{1/2} - \varepsilon_3(1+z_{2,b}^2)^{1/2}}{\varepsilon_2(1+z_{3,b}^2)^{1/2} + \varepsilon_3(1+z_{2,b}^2)^{1/2}} \\ & \times \frac{\varepsilon_1(1+z_{2,a}^2)^{1/2} - \varepsilon_2(1+z_{1,a}^2)^{1/2}}{\varepsilon_1(1+z_{2,a}^2)^{1/2} + \varepsilon_2(1+z_{1,a}^2)^{1/2}} \\ & \sim e^{-2\sqrt{\nu^2/a^2 + \varepsilon_2\zeta_n^2}d} \frac{\varepsilon_2\sqrt{\nu^2/a^2 + \varepsilon_3\zeta_n^2} - \varepsilon_3\sqrt{\nu^2/a^2 + \varepsilon_2\zeta_n^2}}{\varepsilon_2\sqrt{\nu^2/a^2 + \varepsilon_3\zeta_n^2} + \varepsilon_3\sqrt{\nu^2/a^2 + \varepsilon_2\zeta_n^2}} \\ & \times \frac{\varepsilon_1\sqrt{\nu^2/a^2 + \varepsilon_2\zeta_n^2} - \varepsilon_2\sqrt{\nu^2/a^2 + \varepsilon_1\zeta_n^2}}{\varepsilon_1\sqrt{\nu^2/a^2 + \varepsilon_2\zeta_n^2} + \varepsilon_2\sqrt{\nu^2/a^2 + \varepsilon_1\zeta_n^2}}. \quad (19) \end{aligned}$$

By making the substitution $\nu/a \rightarrow k$ and correspondingly $\nu/a^2 \rightarrow dkk$, the Casimir free energy per unit area can be expressed in terms of an integral over k as

$$\begin{aligned} f_{H,s} \sim T \sum_{n=0}^{\infty} \int_0^{\infty} \frac{dkk}{2\pi} \ln \left(1 + \frac{\varepsilon_2\tilde{\kappa}_{3,n} - \varepsilon_3\tilde{\kappa}_{2,n}}{\varepsilon_2\tilde{\kappa}_{3,n} + \varepsilon_3\tilde{\kappa}_{2,n}} \right. \\ \left. \times \frac{\varepsilon_1\tilde{\kappa}_{2,n} - \varepsilon_2\tilde{\kappa}_{1,n}}{\varepsilon_1\tilde{\kappa}_{2,n} + \varepsilon_2\tilde{\kappa}_{1,n}} e^{-2\tilde{\kappa}_{2,n}d} \right), \quad (20) \end{aligned}$$

in which $\tilde{\kappa}_{i,n} = \sqrt{k^2 + \varepsilon_i\zeta_n^2}$, and the Casimir-Lifshitz free energy per unit area for the planar three-layer configuration is thus exactly derived.

APPENDIX: CASIMIR ENERGY OF MULTI-LAYER CONCENTRIC CONFIGURATIONS

The Casimir energy of a concentric system is (The natural unit $\hbar = c = \varepsilon_0 = \mu_0 = k_B = 1$ is used.)

$$\begin{aligned} E^{\text{TE}} = - \sum_{l=1}^{\infty} \nu \int \frac{d\zeta}{2\pi} \frac{1}{W_E} \left[\frac{\mathbf{e}'_+(r)}{\mu(r)} \frac{\partial \zeta \mathbf{e}_-(r)}{\partial \zeta} \right. \\ \left. - \zeta \mathbf{e}_+(r) \frac{\partial}{\partial \zeta} \frac{\mathbf{e}'_-(r)}{\mu(r)} \right]_0^{\infty}, \quad (21) \end{aligned}$$

and the TM contributions are obtained by making the EM-substitutions $\varepsilon \leftrightarrow \mu$, $\mathbf{e} \leftrightarrow \mathbf{h}$, which satisfy

$$\left[\frac{d}{dr} \mu^{-1} \frac{d}{dr} - \frac{l(l+1)}{\mu r^2} - \varepsilon \zeta^2 \right] \mathbf{e}_{\pm}(\zeta, l; r) = 0, \quad (22)$$

$$\left[\frac{d}{dr} \varepsilon^{-1} \frac{d}{dr} - \frac{l(l+1)}{\varepsilon r^2} - \mu \zeta^2 \right] \mathbf{h}_{\pm}(\zeta, l; r) = 0, \quad (23)$$

with + and - signifying the solution being 0 and finite at the infinity and origin, respectively. Within a uniform background, the solutions are denoted as $\mathbf{f}_{\pm}(\zeta, l; r) =$

$\mathbf{e}_{\pm}(\zeta, l; \kappa r) = \mathbf{h}_{\pm}(\zeta, l; \kappa r)$, and $\kappa = \sqrt{\varepsilon \mu} |\zeta|$. Then, for a layered concentric system with the permittivity and permeability being

$$(\varepsilon, \mu)(r) = \begin{cases} (\varepsilon_1, \mu_1), & r < a_1, \\ (\varepsilon_2, \mu_2), & a_1 < r < a_2, \\ \vdots & \vdots \\ (\varepsilon_N, \mu_N), & a_{N-1} < r < a_N, \\ (\varepsilon_{N+1}, \mu_{N+1}), & r > a_N, \end{cases} \quad (24)$$

the solutions, for instance \mathbf{e}_{\pm} , are

$$\mathbf{e}_+(r) = \begin{cases} A_1 \mathbf{f}_{1,+}(r) + B_1 \mathbf{f}_{1,-}(r), & r < a_1, \\ A_2 \mathbf{f}_{2,+}(r) + B_2 \mathbf{f}_{2,-}(r), & a_1 < r < a_2, \\ \vdots & \vdots \\ A_N \mathbf{f}_{N,+}(r) + B_N \mathbf{f}_{N,-}(r), & a_{N-1} < r < a_N, \\ \mathbf{f}_{N+1,+}(r), & r > a_N, \end{cases} \quad \mathbf{e}_-(r) = \begin{cases} \mathbf{f}_{1,-}(r), & r < a_1, \\ C_2 \mathbf{f}_{2,+}(r) + D_2 \mathbf{f}_{2,-}(r), & a_1 < r < a_2, \\ \vdots & \vdots \\ C_N \mathbf{f}_{N,+}(r) + D_N \mathbf{f}_{N,-}(r), & a_{N-1} < r < a_N, \\ C_{N+1} \mathbf{f}_{N+1,+}(r) + D_{N+1} \mathbf{f}_{N+1,-}(r), & r > a_N, \end{cases} \quad (25)$$

The matching conditions leads us to the recursive expressions for those coefficients, taking \mathbf{e}_{\pm} as the instance without losing any generity, above as

$$A_i = A_{i+1} \frac{[\mathbf{f}_{i+1,+}, \mathbf{f}_{i,-}]_{\mu}(a_i)}{W_i} + B_{i+1} \frac{[\mathbf{f}_{i+1,-}, \mathbf{f}_{i,-}]_{\mu}(a_i)}{W_i}, \quad B_i = A_{i+1} \frac{[\mathbf{f}_{i,+}, \mathbf{f}_{i+1,+}]_{\mu}(a_i)}{W_i} + B_{i+1} \frac{[\mathbf{f}_{i,+}, \mathbf{f}_{i+1,-}]_{\mu}(a_i)}{W_i}, \quad (26a)$$

$$A_N = \frac{[\mathbf{f}_{N+1,+}, \mathbf{f}_{N,-}]_{\mu}(a_N)}{W_N}, \quad B_N = \frac{[\mathbf{f}_{N,+}, \mathbf{f}_{N+1,+}]_{\mu}(a_N)}{W_N}, \quad (26b)$$

$$C_{i+1} = C_i \frac{[\mathbf{f}_{i,+}, \mathbf{f}_{i+1,-}]_{\mu}(a_i)}{W_{i+1}} + D_i \frac{[\mathbf{f}_{i,-}, \mathbf{f}_{i+1,-}]_{\mu}(a_i)}{W_{i+1}}, \quad D_{i+1} = C_i \frac{[\mathbf{f}_{i+1,+}, \mathbf{f}_{i,+}]_{\mu}(a_i)}{W_{i+1}} + D_i \frac{[\mathbf{f}_{i+1,+}, \mathbf{f}_{i,-}]_{\mu}(a_i)}{W_{i+1}}, \quad (26c)$$

$$C_2 = \frac{[\mathbf{f}_{1,-}, \mathbf{f}_{2,-}]_{\mu}(a_1)}{W_2}, \quad D_2 = \frac{[\mathbf{f}_{2,+}, \mathbf{f}_{1,-}]_{\mu}(a_1)}{W_2}. \quad (26d)$$

For example, $N = 2$ case can be written as

$$A_1 = \frac{[\mathbf{f}_{3,+}, \mathbf{f}_{2,-}]_{\mu}(a_2)}{W_2} \frac{[\mathbf{f}_{2,+}, \mathbf{f}_{1,-}]_{\mu}(a_1)}{W_1} + \frac{[\mathbf{f}_{2,+}, \mathbf{f}_{3,+}]_{\mu}(a_2)}{W_2} \frac{[\mathbf{f}_{2,-}, \mathbf{f}_{1,-}]_{\mu}(a_1)}{W_1}, \quad (27a)$$

$$A_2 = \frac{[\mathbf{f}_{3,+}, \mathbf{f}_{2,-}]_{\mu}(a_2)}{W_2}, \quad B_2 = \frac{[\mathbf{f}_{2,+}, \mathbf{f}_{3,+}]_{\mu}(a_2)}{W_2}, \quad (27b)$$

$$D_3 = \frac{[\mathbf{f}_{1,-}, \mathbf{f}_{2,-}]_{\mu}(a_1)}{W_2} \frac{[\mathbf{f}_{3,+}, \mathbf{f}_{2,+}]_{\mu}(a_2)}{W_3} + \frac{[\mathbf{f}_{2,+}, \mathbf{f}_{1,-}]_{\mu}(a_1)}{W_2} \frac{[\mathbf{f}_{3,+}, \mathbf{f}_{2,-}]_{\mu}(a_2)}{W_3}, \quad (27c)$$

$$C_2 = \frac{[\mathbf{f}_{1,-}, \mathbf{f}_{2,-}]_{\mu}(a_1)}{W_2}, \quad D_2 = \frac{[\mathbf{f}_{2,+}, \mathbf{f}_{1,-}]_{\mu}(a_1)}{W_2}, \quad (27d)$$

$$E^{\text{TE}} = \sum_{l=1}^{\infty} \nu \int \frac{d\zeta}{2\pi} \ln D_3 = \sum_{l=1}^{\infty} \nu \int \frac{d\zeta}{2\pi} \ln \left\{ 1 - \frac{[\mathbf{f}_{3,+}, \mathbf{f}_{2,+}]_{\mu}(a_2) [\mathbf{f}_{2,-}, \mathbf{f}_{1,-}]_{\mu}(a_1)}{[\mathbf{f}_{3,+}, \mathbf{f}_{2,-}]_{\mu}(a_2) [\mathbf{f}_{2,+}, \mathbf{f}_{1,-}]_{\mu}(a_1)} \right\}, \quad (27e)$$

where the bulk terms are subtracted in the first step, and the surface divergence is subtracted in the second step. To find D_{N+1} , we write

$$\begin{bmatrix} C_{i+1} \\ D_{i+1} \end{bmatrix} = M_{i+1,i} \begin{bmatrix} C_i \\ D_i \end{bmatrix} = \begin{bmatrix} \frac{[f_{i,+},f_{i+1,-}]_\mu(a_i)}{W_{i+1}} & \frac{[f_{i,-},f_{i+1,-}]_\mu(a_i)}{W_{i+1}} \\ \frac{[f_{i+1,+},f_{i,+}]_\mu(a_i)}{W_{i+1}} & \frac{[f_{i+1,+},f_{i,-}]_\mu(a_i)}{W_{i+1}} \end{bmatrix} \begin{bmatrix} C_i \\ D_i \end{bmatrix}, \quad (28a)$$

which gives us

$$E^{\text{TE}} = \sum_{l=1}^{\infty} \nu \int \frac{d\zeta}{2\pi} \ln D_{N+1} = \sum_{l=1}^{\infty} \nu \int \frac{d\zeta}{2\pi} \ln \left\{ 1 + \frac{M_{N+1,N}^{2,j_N} \cdots M_{i+1,i}^{j_{i+1},j_i} \cdots M_{2,1}^{j_2,2}}{M_{N+1,N}^{2,2} \cdots M_{i+1,i}^{2,2} \cdots M_{2,1}^{2,2}} \right\}. \quad (28b)$$

The corresponding TM contribution can be obtained in the same way.

ACKNOWLEDGMENTS

We thank the Terahertz Physics and Devices Group, Nanchang University for the strong computational facility support. Y.L. was supported by the National Natural Science Foundation of China (Grant No. 12304396). P.P. thanks T. Jayasekara for collaborative assistance during the course of this work. The research by O.I.M. and M.B. is part of Project No. 2022/47/P/ST3/01236 co-funded by the National Science Centre and the European Union’s Horizon 2020 research and innovation program under the Marie Skłodowska-Curie Grant Agreement No. 945339. Institutional and infrastructural support for the ENSEMBLE3 Centre of Excellence was provided

through the ENSEMBLE3 project (MAB/2020/14) delivered within the Foundation for Polish Science International Research Agenda Programme and co-financed by the European Regional Development Fund and the Horizon 2020 Teaming for Excellence initiative (Grant Agreement No. 857543), as well as the Ministry of Education and Science initiative “Support for Centres of Excellence in Poland under Horizon 2020”. We gratefully acknowledge Poland’s high-performance computing infrastructure PLGrid (HPC Centers: ACK Cyfronet AGH) for providing computer facilities and support within computational Grant No. PLG/2023/016228. C.P. thanks the European Union’s Horizon 2020 research and innovation program (GA No. 101058694).

* leon@ncu.edu.cn

† Prachi.Parashar@jalc.edu

‡ mathias.bostrom@ensemble3.eu

¹ J. Mülmenstädt, O. Sourdeval, J. Delanoë, and J. Quaas, “Frequency of occurrence of rain from liquid-, mixed-, and ice-phase clouds derived from a-train satellite retrievals,” *Geophys. Res. Lett.* **42**, 6502–6509 (2015).

² T. Storelvmo and I. Tan, “The Wegener-Bergeron-Findeisen process - Its discovery and vital importance for weather and climate,” *Meteorol. Zeitschrift* **24**, 455–461 (2015).

³ M. Arienti, M. Geier, X. Yang, J. Orcutt, J. Zenker, and S. D. Brooks, “An experimental and numerical study of the light scattering properties of ice crystals with black carbon inclusions,” *J. Quant. Spectrosc. Radiat. Transf.* **211**, 50–63 (2018).

⁴ X. Zeng, W. K. Tao, M. Zhang, A. Y. Hou, S. Xie, S. Lang, X. Li, D. O’C Starr, X. Li, and J. Simpson, “An indirect effect of ice nuclei on atmospheric radiation,” *J. Atmos. Sci.* **66**, 41–61 (2009).

⁵ R. E. Hawker, A. K. Miltenberger, J. M. Wilkinson, A. A. Hill, B. J. Shipway, Z. Cui, R. J. Cotton, K. S. Carslaw, P. R. Field, and B. J. Murray, “The temperature dependence of ice-nucleating particle concentrations affects the radiative properties of tropical convective cloud systems,” *Atmos. Chem. Phys.* **21**, 5439–5461 (2021).

⁶ S. M. Burrows, C. S. McCluskey, G. Cornwell, I. Steinke, K. Zhang, B. Zhao, M. Zawadowicz, A. Raman, G. Kulka-

rni, S. China, A. Zelenyuk, and P. J. DeMott, “Ice-Nucleating Particles That Impact Clouds and Climate: Observational and Modeling Research Needs,” *Rev. Geophys.* **60**, e2021RG000745 (2022).

⁷ N. Maeda, “Brief overview of ice nucleation,” *Molecules* **26**, 392 (2021).

⁸ W. Findeisen, E. Volken, A. M. Giesche, and S. Brönnimann, “Colloidal meteorological processes in the formation of precipitation,” *Meteorol. Zeitschrift* **24**, 443–454 (2015).

⁹ G. Vali, “Sizes of atmospheric ice nuclei,” *Nature* **212**, 384–385 (1966).

¹⁰ J. D. Atkinson, B. J. Murray, M. T. Woodhouse, T. F. Whale, K. J. Baustian, K. S. Carslaw, S. Dobbie, D. O’Sullivan, and T. L. Malkin, “The importance of feldspar for ice nucleation by mineral dust in mixed-phase clouds,” *Nature* **498**, 355–358 (2013).

¹¹ B. J. Murray, “Cracking the problem of ice nucleation,” *Science* **355**, 346–347 (2017).

¹² A. Kiselev, F. Bachmann, P. Pedevilla, S. J. Cox, A. Michaelides, D. Gerthsen, and T. Leisner, “Active sites in heterogeneous ice nucleation—the example of k-rich feldspars,” *Science* **355**, 367–371 (2017).

¹³ G. Lloyd, T. Choularton, K. Bower, J. Crosier, M. Gallagher, M. Flynn, J. Dorsey, D. Liu, J. W. Taylor, O. Schlenker, J. Fugal, S. Borrmann, R. Cotton, P. Field, and A. Blyth, “Small ice particles at slightly supercooled temperatures in tropical maritime convection,”

- Atmos. Chem. Phys.* **20**, 3895–3904 (2020).
- ¹⁴ J. L. Aragonés, L. G. MacDowell, and C. Vega, “Dielectric constant of ices and water: A lesson about water interactions,” *J. Phys. Chem. A* **115**, 5745–5758 (2011).
 - ¹⁵ J. Fiedler, M. Boström, C. Persson, I. H. Brevik, R. W. Corkery, S. Y. Buhmann, and D. F. Parsons, “Full-spectrum high resolution modeling of the dielectric function of water,” *J. Phys. Chem. B* **124**, 3103–3113 (2020).
 - ¹⁶ J. Luengo-Márquez and L. G. MacDowell, “Lifshitz theory of wetting films at three phase coexistence: The case of ice nucleation on silver iodide (agi),” *J. Coll. Interf. Sci.* **590**, 527–538 (2021).
 - ¹⁷ J. Luengo-Marquez, F. Izquierdo-Ruiz, and L. G. MacDowell, “Intermolecular forces at ice and water interfaces: Premelting, surface freezing, and regelation,” *J. Chem. Phys.* **157**, 044704 (2022).
 - ¹⁸ M. Elbaum and M. Schick, “On the failure of water to freeze from its surface,” *J. Phys. I France* **1**, 1665–1668 (1991).
 - ¹⁹ M. Elbaum and M. Schick, “Application of the theory of dispersion forces to the surface melting of ice,” *Phys. Rev. Lett.* **66**, 1713–1716 (1991).
 - ²⁰ P. Parashar, K. V. Shajesh, K. A. Milton, D. F. Parsons, I. Brevik, and M. Boström, “Role of zero point energy in promoting ice formation in a spherical drop of water,” *Phys. Rev. Research* **1**, 033210 (2019).
 - ²¹ Kimball A Milton, “Semiclassical electron models: Casimir self-stress in dielectric and conducting balls,” *Ann. Phys. (N.Y.)* **127**, 49–61 (1980).
 - ²² Philip Candelas, “Vacuum energy in the presence of dielectric and conducting surfaces,” *Ann. Phys. (N.Y.)* **143**, 241–295 (1982).
 - ²³ I Brevik and H Kolbenstvedt, “Electromagnetic Casimir densities in dielectric spherical media,” *Ann. Phys. (N.Y.)* **149**, 237–253 (1983).
 - ²⁴ Iver Brevik and G. H. Nyland, “Casimir force on a dielectric cylinder,” *Ann. Phys. (N.Y.)* **230**, 321–342 (1994).
 - ²⁵ Yael Avni and Ulf Leonhardt, “Casimir self-stress in a dielectric sphere,” *Ann. Phys. (N.Y.)* **395**, 326–340 (2018).
 - ²⁶ Kimball A Milton, Prachi Parashar, Iver Brevik, and Gerard Kennedy, “Self-stress on a dielectric ball and Casimir-Polder forces,” *Ann. Phys. (N.Y.)* **412**, 168008 (2020).
 - ²⁷ Kimball A Milton and Iver Brevik, “Casimir energies for isorefractive or diaphanous balls,” *Symmetry* **10**, 68 (2018).
 - ²⁸ Yang Li, “Casimir stresses of the dielectric ball: inhomogeneity and divergences,” arXiv preprint arXiv:2411.07911 (2024).
 - ²⁹ E. M. Lifshitz, “The theory of molecular attractive forces between solids,” *Sov. Phys. JETP* **2**, 73 (1956).
 - ³⁰ I. E. Dzyaloshinskii, E. M. Lifshitz, and L. P. Pitaevskii, “The general theory of van der Waals forces,” *Adv. Phys.* **10**, 165 (1961).
 - ³¹ M. Boström, V. Estesó, J. Fiedler, I. Brevik, S. Y. Buhmann, C. Persson, S. Carretero-Palacios, D. F. Parsons, and R. W. Corkery, “Self-preserving ice layers on CO₂ clathrate particles: Implications for Enceladus, Pluto, and similar ocean worlds,” *Astron. Astrophys.* **650**, A54 (2021).
 - ³² M. Kerker, [The scattering of light and electromagnetic radiation](#) (Academic Press, New York, 1969).
 - ³³ V. Estesó, S. Carretero-Palacios, L. G. MacDowell, J. Fiedler, D. F. Parsons, F. Spallek, H. Míguez, C. Persson, S. Y. Buhmann, I. Brevik, and M. Boström, “Premelting of ice adsorbed on a rock surface,” *Phys. Chem. Chem. Phys.* **22**, 11362–11373 (2020).
 - ³⁴ Y. Li, K. A. Milton, I. Brevik, O. I. Mal’yi, P. Thiyam, C. Persson, D. F. Parsons, and M. Boström, “Premelting and formation of ice due to Casimir-Lifshitz interactions: Impact of improved parameterization for materials,” *Phys. Rev. B* **105**, 014203 (2022).
 - ³⁵ P. Thiyam, J. Fiedler, S. Y. Buhmann, C. Persson, I. Brevik, M. Boström, and D. F. Parsons, “Ice Particles Sink below the Water Surface Due to a Balance of Salt, van der Waals, and Buoyancy Forces,” *J. Phys. Chem. C* **122**, 15311–15317 (2018).
 - ³⁶ R. E. Stoiber, S. N. Williams, and B. Huebert, “Annual contribution of sulfur dioxide to the atmosphere by volcanoes,” *J. Volcanol. Geotherm. Res.* **33**, 1–8 (1987).
 - ³⁷ D. F. Parsons and A. Salis, “The impact of the competitive adsorption of ions at surface sites on surface free energies and surface forces,” *J. Chem. Phys.* **142**, 134707 (2015).
 - ³⁸ D. F. Parsons, C. Carucci, and A. Salis, “Buffer-specific effects arise from ionic dispersion forces,” *Phys. Chem. Chem. Phys.* **24**, 6544–6551 (2022).
 - ³⁹ H. R. Pruppacher and J. D. Klett, [Microphysics of Clouds and Precipitation](#), Atmospheric and Oceanographic Sciences Library (Springer Dordrecht, 2010).
 - ⁴⁰ D. A. Knopf and P. A. Alpert, “Atmospheric ice nucleation,” *Nat. Rev. Phys.* **5**, 203–217 (2023).
 - ⁴¹ F. W. J. Olver, [NIST handbook of mathematical functions hardback and](#) (Cambridge university press, 2010).